

# The physicochemical and biological properties of novel silver nanoparticles synthesized by the extract of *Holigarna ferruginea*

Kumbar Mudakappa Manjunath\*, Y. L. Krishnamurthy

Department of Applied Botany, Kuvempu University, Shivamogga, Karnataka, India.

## ARTICLE INFO

### Article history:

Received on: November 25, 2022

Accepted on: February 04, 2023

Available online: April 04, 2023

### Key words:

Green synthesis,  
*Holigarna ferruginea*,  
Characterization,  
Cyclic voltammetry,  
Antibacterial,  
Anticancer.

## ABSTRACT

The green synthesis of silver nanoparticles (AgNPs) by the extract of *Holigarna ferruginea*, due to its potential widespread biomedical applications; nanoparticles were set the remarkable application in the medical field and show antibacterial and anti-cancerous properties. UV-visible spectrophotometer (UV), Fourier-transform infrared spectroscopy (FTIR), X-ray diffraction (XRD), and scanning electron microscopy (SEM) were used to characterize the nanoparticles, and cyclic voltammetry (CV) reveals the physicochemical properties of the nanoparticles. After the color-changing, the synthesis process was confirmed by UV-visible spectrophotometer, and the absorption peak was reported at 418 nm, the functional groups, and the crystallite nature of particles were confirmed by FTIR and XRD, respectively. While, the morphological study was done by SEM and reports the spherical-shaped particles, and the cyclic volta-gram disclosed the radical scavenging properties. The antibacterial agent enhanced the antibacterial activity of the nanomaterial and reported a concentration-dependent zone of inhibition. The AgNPs reported about  $15.33 \pm 0.57$  mm of a zone of inhibition in *Staphylococcus aureus* and about  $14.66 \pm 0.57$  mm of a zone of inhibition in *Klebsiella pneumoniae* at the highest concentration of about 1000  $\mu\text{g/ml}$ . The AgNPs reported dose-dependent anticancer activity in women's breast cancer cell lines (MCF-7). The MTT study revealed a dose-dependent toxic nature, with approximately 44% cell viability at 50  $\mu\text{g/ml}$  concentration, likewise, 13% of cell viability at 400  $\mu\text{g/ml}$ .

## 1. INTRODUCTION

Nanotechnology is a new and emerging branch of science because it has some distinctive properties, such as physical, chemical, electronic, and bioactive properties [1]. In general, nanoparticles are crystalline grains of nature having 5–100 nm in size with a prominent surface area, the non-nanomaterials have less surface area than nanoparticles, because of their size and surface area, the nanoparticles show prominent applications in various field [2] in medicine [3], and antibacterial activity [4]. The plant-mediated nanoparticles are a more focused and emerging research objective in nanotechnology, especially the silver nanoparticle which have their special trademark in daily used consumer products [5]. There are some standard methods for the synthesis of nanoparticles, namely, top-down or bottom-up approaches (physical method, chemical method, and biological method) from each method they synthesize nanoparticles with different properties such as size, shape, surface, chemical properties magnetic properties, and medicinal properties [6]. In plant-mediated silver nanoparticles (AgNPs), biomolecules such as vitamins, amino acids, polysaccharides, proteins,

phenolics, saponins, and alkaloids play a major role as biological reducing, capping, and stabilizing agents [7,8]. Due to their distinctive features and distinctive mode of therapeutic action as antibacterial and anticancer agents, the environmentally safe and economically advantageous green synthesized AgNPs are extensively used [9]. Green synthesis of AgNPs is one of the best successful scientific methods. AgNPs are known as antibacterial agents in the field of nanomedicine because they inhibit microbial contact and contamination [10]. Moreover, the physical techniques need expensive equipment, high temperatures, and high pressures. Toxic substances that may seriously harm the environment and living things are used in the chemical creation of nanoparticles and are non-eco-friendly. These drawbacks restrict the utilization of physical and chemical techniques. Green synthesis, which is more cost-effective and ecologically beneficial than these technologies, has taken its place. The green production of nanoparticles often uses plants, bacteria, fungi, algae, etc. Many studies have documented the green production of AgNPs from plant extracts from various plant parts, including peel, leaves, roots, stems, and fruit [9]. Because plants are the natural source of reducing and capping agents such as phenols, glycosides, and polysaccharides, they are essential molecules that influence particle shape and size [11]. Plants are nature's chemical factory, and nanotechnology or nanoparticles are good for drug delivery and action. These are the main reasons to study green synthesis. The species *Holigarna ferruginea* is one of the semi-evergreen and evergreen medium-sized tree species and contains black

\*Corresponding Author:

Kumbar Mudakappa Manjunath

Department of Applied Botany, Kuvempu University, Shivamogga, Karnataka, India.

E-mail: [kmanjunathm1@gmail.com](mailto:kmanjunathm1@gmail.com)

acid juice, which causes skin dermatitis [12]. The other species of the genus *Holigarna* shows some bioactive properties and has been reported [13-17]. Recently Lokapur *et al.* [18] reported bioactive properties (antioxidant and anticancer) of Zinc oxide nanoparticles synthesized by *Holigarna grahamii*, based on these previous reports and articles, the genus *Holigarna* shows promising phytochemical properties, but the reports are less in number with respect to green synthesis, for this reason, we chose *H. ferruginea* as a working sample to assess their binding and stabilizing capacity during silver nanoparticle synthesis, as well as their bioactive properties such as antibacterial and anticancer properties.

## 2. MATERIALS AND METHODS

### 2.1. Chemicals

Silver nitrate ( $\text{AgNO}_3$ ) and dimethyl sulfoxide (DMSO) were purchased from Merck, nutrient agar, and Mueller-Hinton agar (MHA) media, cetyltrimethylammonium bromide (CTAB) and agarose were purchased from Hi Media, ampicillin from Cipla, phosphate buffer saline was purchased from Hi Media, ethanol and methanol (analytic grade reagents) were purchased and used.

### 2.2. Plant Collection

The genus *Holigarna* is a large and lofty evergreen tree with acid juice in the stem and leaves. About eight species have been reported from India and Indochina [19], and they are endemic to the Western Ghats, common from the South to the Central Sahyadri, and rare in the North Sahyadri. Low-elevation canopy trees in semi-evergreen to wet evergreen forests [13]. The plant samples were collated from the Bisle Ghat ( $12^\circ 42' 42''$  N:  $75^\circ 41' 17''$  E) one of the evergreen forest regions in Hassan District, Karnataka, India. The plant and collection site was shown in Figure 1.

### 2.3. Plant Identification by Morphomolecular Approach

The collected sample material was identified based on morphomolecular approaches. The plant was identified based on the morphological key characteristics such as acid juice, phyllotaxy, lateral secondary venation, spurs, panicle color, and flower type [20] and the herbarium

was submitted to the department of Botany Kuvempu University as shown in Figure 2, and the voucher number is KUAB479. The molecular approach is purely marker-based, here the modified CTAB method was used for DNA isolation [21]. A 0.8% agarose gel was used to examine the genomic DNA recovered. There were no errors in any of the polymer chain reaction amplification reaction components, and a standard polymer chain reaction mixture was modified as 25 ml of PCR reaction mixture was prepared using 1.5 ml primers, 2.5 ml of dNTP's, 2.5 ml PCR buffer with 15 mM  $\text{MgCl}_2$ , 2 ml template DNA, 0.3 units/25 ml reaction mixture of Taq polymerase (Stock 3 u/ml), and volume made up to 25 ml with sterile water. Moreover, we employed the ITS1-TCCGTAGGTGAACCTCGG and ITS 2-GCTGCGTTCTTCATCGATGC nuclear regions [22]. For PCR amplification an initial denaturation stage at  $94^\circ\text{C}$  for 2 min, followed by 25 cycles of  $94^\circ\text{C}$  for 30 s,  $55^\circ\text{C}$  for 30 s,  $72^\circ\text{C}$  for 45 s followed by a final extension at  $72^\circ\text{C}$  for 10 min. Sequencing of amplified products took place by applied bioscience. Submissions for National Centre for Biotechnology Information GenBank were also made, the submitted (ingroup) and other outgroup archived accessions are listed in Table 1, and the distance matrix technique unweighted pair group method with arithmetic mean (UPGMA) was used to build the phylogenetic tree.

### 2.4. Preparation of Sample

The fresh *H. ferruginea* sample was collected, washed twice with tap water and sterile distilled water, and kept for shady dry for about 3 days in an aseptic condition. The sample was chopped and grinded in mechanical machines and got clean and fine powder, about 10 g of powder was added to the beaker containing 200 ml of sterile double-distilled water. The mixture was kept and allowed for boiling in a water bath for about 20 min at  $60^\circ\text{C}$  to separate the phytochemical constituents from the powder, the solution was filtered through a 0.2  $\mu\text{m}$  membrane, and the filtered solution was centrifuged at 5000 rpm for about 5 min then the solution was filtered by Whatman filter paper. The filtrate was kept at  $4^\circ\text{C}$  for the future studies.

### 2.5. Synthesis of Nanoparticles

A standard and exact 1000 ml of 1 mM  $\text{AgNO}_3$  was prepared. The previously prepared plant extract or filtrate was added to a clean

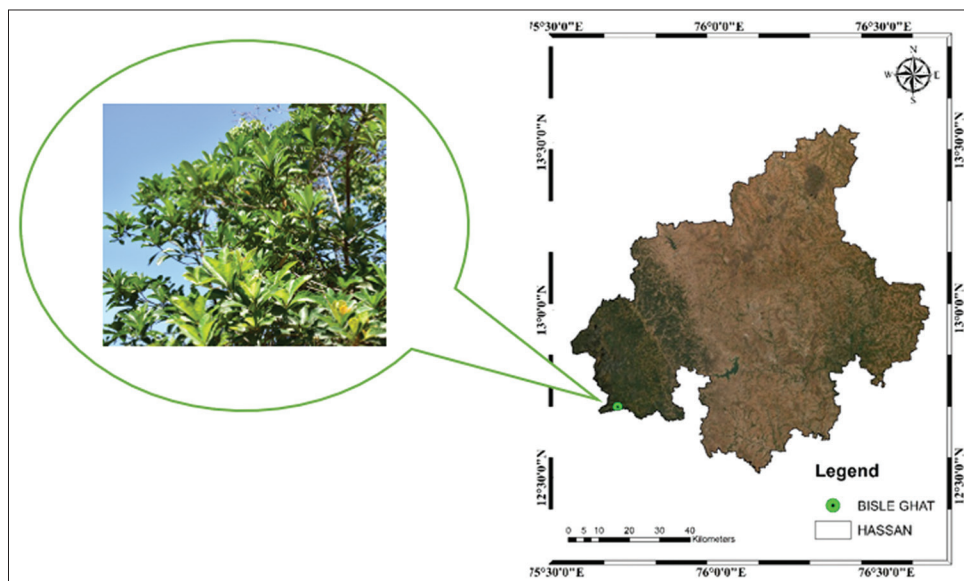


Figure 1: Plant specimen and collecting site of *Holigarna ferruginea*.



Figure 2: Herbarium specimen of *Holigarna ferruginea*.

Table 1: Archived data for phylogenetic tree construction.

S. No	Plant taxon	GenBank accession number	Submitted by
1	<i>Holigarna ferruginea</i>	OK284371	K Manjunath and Y.L Krishnamurthy
2	<i>Holigarna arnottiana</i>	OK235482	K Manjunath and Y.L Krishnamurthy
3	<i>Holigarna beddomei</i>	OK284370	K Manjunath and Y.L Krishnamurthy
4	<i>Holigarna grahamii</i>	OM010328	K Manjunath and Y.L Krishnamurthy
5	<i>Holigarna nigra</i>	OK284373	K Manjunath and Y.L Krishnamurthy
6	<i>Schinus terebinthifolius</i>	KF420944	Bolson, M
7	<i>Searsia lucida</i>	EF682851	Pell, S.K.
8	<i>Searsia lancea</i>	EF682850	Pell, S. K
9	<i>Searsia tenuinervis</i>	KX360048	Yang, Y. Y
10	<i>Toxicodendron succedaneum</i>	KP093195	Liu, J
11	<i>Toxicodendron succedaneum</i>	KP093196	Liu, J
12	<i>Pistacia chinensis</i>	DQ390466	Miller, A. J
13	<i>Pistacia chinensis</i>	MH711767	Zeng, C
14	<i>Rhus michauxii</i>	AY641488	Miller, A. J
15	<i>Rhus lanceolata</i>	AY641487	Miller, A. J

conical flask containing the known standard precursor ( $\text{AgNO}_3$ ) in the ratio of 1:9 (100 ml plant extract + 900 ml of  $\text{AgNO}_3$ ), this whole setup was done on a magnetic stirrer and incubated at the dark condition to avoid photoactivation of  $\text{AgNO}_3$  with a pH of 9.5. After the incubation period, the color developed from light yellowish to thick dark brown, and the synthesis of nanoparticles was observed as shown in Figure 3. After the color developed, the final reaction mixture was transferred to centrifuge tubes, the mixture was centrifuged at 10,000 rpm for 30 min, the supernatant was discarded and the pellet was centrifuged with 20 ml of sterile double-distilled water at 8000 rpm for 20 min, the supernatant was discarded and the pellet was centrifuged and washed with 90% of 10 ml ethanol at 5000 rpm for 5 min, finally, the supernatant was discarded and the dried pellet was collected [1,23].

## 2.6. Characterization of Synthesized AgNPs

Before they may be employed for their intended purpose, the synthesis of AgNPs must be first confirmed by certain techniques. The simplest way for monitoring AgNPs production is to visually observe the color changes in the solution from simple yellow to dark brown. UV-visible spectroscopic analysis of the sample was done using Perkin Elmer Lambda 750 instrument and measurements were conducted at the wavelength of 250–600 nm. Fourier-transform infrared spectroscopy (FTIR) spectroscopy may aid in the identification of biomolecules that impact nanoparticle production and stability, measurements were analyzed in the range of 400–4000  $\text{cm}^{-1}$ , with Parkin Elmer Spectrum 1000. X-ray diffraction (XRD) of AgNPs was analyzed using Rigaku Smart lab with an operating current at 30 mA and a voltage of 40 kV, and scanning was done at  $2\theta$  from  $20^\circ$  to  $80^\circ$ . Furthermore, the scanning electron microscopy (SEM) of the TESCAN Bruker instrument was used to analyze the morphological characters of AgNPs [24].

## 2.7. Radical Scavenger Analysis by Cyclic Voltammetry (CV)

The radical scavenging property of green synthesized AgNPs was carried out by the cyclic voltameter. The electrochemical analysis of the selected AgNPs was analyzed by an Electrochemical workstation CHI 600 c, the measurements were generated using a conventional three-electrode system, namely, the saturated calomel (reference electrode), platinum wire (counter electrode), and glossy corban paste electrode (working electrode). The 0.5 g of the synthesized AgNPs was dissolved in 100 ml of methanol for analysis, and 0.2 M phosphate buffer with pH 7.0 was used as the electrolyte. The cyclic voltammetric behavior of quiring simple was recorded at a different scan rate of electric potential from 50 to 300 mV/s [25,26].

## 2.8. Antibacterial Activity

The antibacterial efficacy of AgNPs was analyzed against laboratory control strains of the microbial type cultures (MTCC) obtained from IMTECH Chandigarh. The antibacterial activity was investigated against the Gram-positive bacteria *Staphylococcus aureus* MTCC (3160) and *Klebsiella pneumoniae* MTCC (7407), the Gram-negative bacteria. The bacterial suspension of 18 h grown strains was swabbed on the MHA plates using a cotton swab and allowed to solidify. The wells were made by the sterile borer and filled with 50  $\mu\text{L}$  of AgNPs at three different concentrations (1000, 500, and 250  $\mu\text{g}/\text{mL}$ ), here we used DMSO as a blank, and ampicillin as a standard antibacterial drug. The plates were kept and allowed to incubate at  $37^\circ\text{C}$  for about 18 h, then the zone of inhibition of each well was analyzed and measured [27].

## 2.9. Cytotoxicity by MTT Assay

### 2.9.1. Culture

The Women's breast cancer cell lines were washed twice with phosphate buffer saline (PBS) and centrifuged at 1500 rpm (Revolution per minute) for 3 min, resuspended the pellet in a suitable medium (medium with 10% fetal bovine serum), and plated the cell lines in 96 well plates. The culture cells were incubated at 37°C for 24 h.

### 2.9.2. Cytotoxicity

The anticancer efficacy of AgNPs against MCF-7 (Women's breast cancer cell lines) was carried out by MTT assay, and the previously cultured cells (3000–10000 cells for each well cultured in 96 well plates) were tested with two compounds (AgNPs and one standard cancer medicine cisplatin) in different concentrations for about 48 h. Subsequently, 20 µL of MTT reagent (5 mg/mL in PBS) was added to each reaction and reactions were incubated in a CO<sub>2</sub> incubator for about 4 h at 37°C. Add 100 µl of solubilization solution (DMSO with formazan) to all the wells after the incubation. Allow the plates for overnight incubation and check for complete purple formazan crystals solubilization, then measured and record the absorbance at 570nm by using a multi-well plate reader [28].

## 3. RESULTS AND DISCUSSION

The systematics investigation that used UPGMA revealed that each taxonomic group possessed a single and monophyletic presence. The term "monophyletic" refers to groups of species in which each

taxonomic category derives from a specific single common ancestor and also includes all of the descendants of the common ancestor [29]. Here, the UPGMA tree indicates separate groups of taxa based on a distance matrix, *H. ferruginea* showing a close relation to *Holigarna arnottiana*, *Holigarna beddomei*, and the entire genus, while the rest of the taxonomic groups are grouped and separated with their respective taxa and depicted in Figure 4. Moreover, here, the query taxon was confirmed by systematic grouping or placement or position of *H. ferruginea* with their respective ingroup species such as *H. arnottiana*, *H. grahamii*, *Holigarna nigra*, and *H. beddomei*.

### 3.1. UV-visible Spectrophotometer

As part of the first validation, a UV-visible spectral scan (250–600 nm) was used to further validate the color shift that was seen in the AgNPs samples after the green synthesis. The produced AgNPs strong distinctive absorption peak at 418 nm while the aqueous plant extracts do not show any spectral peaks as shown in Figure 5. The conversion of AgNO<sub>3</sub> to the silver oxide by the extract of *H. ferruginea* is confirmed by the UV data's broad peak absorption. The color was generated by the surface plasmon excitation of metal nanoparticles, and this is the indication of the synthesis of AgNPs [9]. The peaks around 400–450 nm are specific for AgNPs because due to surface plasmon resonance of AgNPs. The conduction electrons undergo oscillation due to the strong interaction of light with the AgNPs [30]. Some results reported in the previous studies showed a resemblance at 450 nm [31], and 440 nm [32].

### 3.2. FTIR Analysis of Synthesized AgNPs

After carrying out the FTIR, we were able to identify the functional groups and are accountable for the capping and effective stability of the plant-mediated AgNPs. Here, 12 major absorbance stretching band peaks were observed as shown in Figure 6. From the single band region, the absorption peak at 3197.4 cm<sup>-1</sup> was assigned to O-H alcohol, 2907.6 cm<sup>-1</sup> represented the C-H alkene, 2664.2 cm<sup>-1</sup> was assigned to O-H, and vibration which may be indicated the presence of carboxylic acid, 2331.1 cm<sup>-1</sup> represents the O=C=O carbon dioxide stretch, 2116.3 cm<sup>-1</sup> represents the C≡C alkene, 1926.1 cm<sup>-1</sup> correspond to the C–H bending vibration of alkanes, 1735.6 cm<sup>-1</sup> represents the C=O conjugated acids, 1539 cm<sup>-1</sup> assigned to N-O stretch it corresponds to the nitro compound and 881.6 cm<sup>-1</sup>, 783.3 cm<sup>-1</sup> represents the



Figure 3: Visual observation of non-synthesized and synthesized AgNPs based on color development.

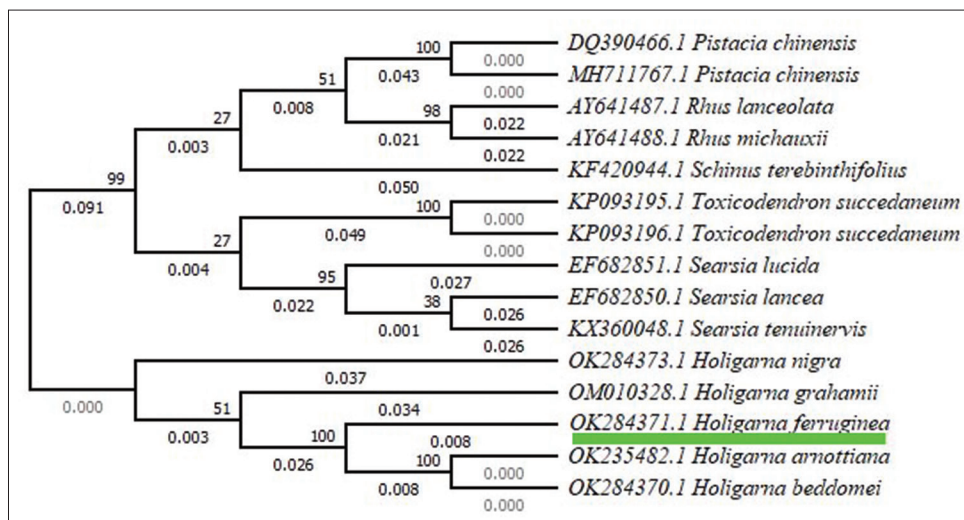
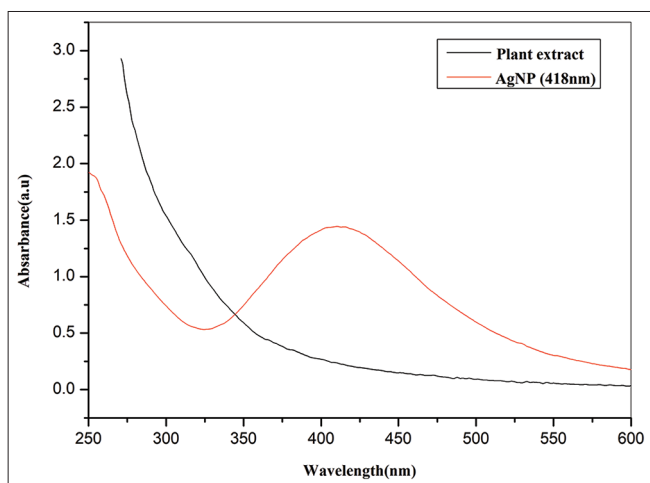


Figure 4: The phylogenetic systematics tree of *Holigarna ferruginea* by distance matrix-based (UPGMA).

C-H bending [33,34]. Furthermore, the study identified probable biomolecules involved in silver bioreduction and AgNPs stability. The formation of stretching and bending vibrations in the 4000–400  $\text{cm}^{-1}$  range is the result of the interaction of non-destructive infrared light with the bonding of synthesized molecules. Because the carbonyl (-CO) and hydroxyl (-OH) functional groups revealed the existence of flavanones or terpenoids adsorbed on the surface of nanoparticles through interactions through  $\pi$ -electrons in the carbonyl groups, they are implicated in the reduction, capping, and stability of AgNPs. It was also established that the carbonyl groups in proteins and amino acids have a greater potential to connect with AgNPs or act as reduction, capping, and stabilizing agents [35,36].

### 3.3. XRD Analysis of AgNPs

For both qualitative and quantitative investigations of nanoparticles, XRD is a potent characterization tool. XRD measurements are used to confirm nanoparticle synthesis and evaluate their crystal structure. Furthermore, this approach has been utilized to compute the size of crystalline nanoparticles and to assess the degree of crystallinity [37]. The XRD pattern of green synthesized AgNPs is depicted in Figure 7.



**Figure 5:** UV-visible spectrum of AgNPs green synthesized by the extract of *Holigarna ferruginea*.

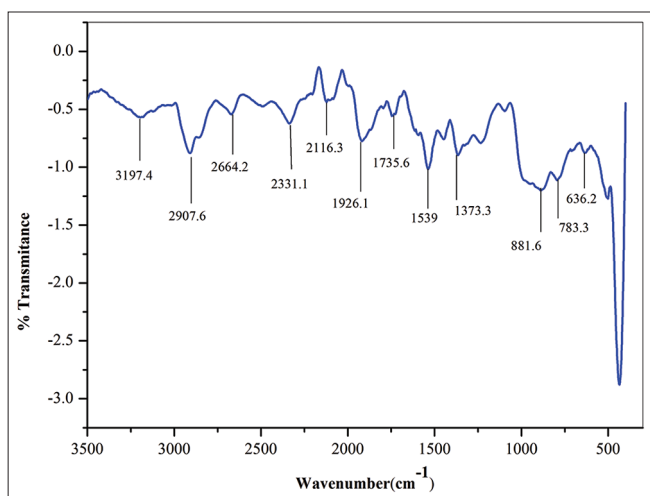


**Figure 6:** FTIR spectrum shows the various peaks of silver nanoparticles synthesized by extract of *Holigarna ferruginea*.

The different peaks indicate the reduction mechanism of  $\text{AgNO}_3$  into silver oxide. The XRD peaks and their corresponded planes are tabulated in Table 2, and a total of nine different peaks were plotted. A number of Bragg reflections is observed at  $2\theta$  values  $27.77^\circ$ ,  $32.19^\circ$ ,  $38.09^\circ$ ,  $44.25^\circ$ ,  $46.20^\circ$ ,  $54.80^\circ$ ,  $57.46^\circ$ ,  $64.47^\circ$ , and  $77.11^\circ$  which corresponds to (210), (122), (111), (200), (231), (142), (241), (220), and (311) planes of pure silver based on the face-centered cubic structure. The following peaks could be assigned to the extract containing the organic compounds which are responsible for reducing and stabilizing the AgNPs and revealed that the structure corresponds to the face-centered cubic crystal of AgNPs [38]. Because the *H. ferruginea* contains certain proteins, and bioorganic chemicals and crystallizes on the surface of the silver, a few unassigned peaks were seen in the XRD pattern [39]. The crystallite nature of particles was calculated by the Bragg equation ( $D=0.9 \lambda/B \cos \theta$ ) and the average crystallite size is 17.28 nm. The JCPDS file No. 04-0783 [40].

### 3.4. SEM Imaging of AgNPs

Among other electron microscopy methods, SEM can analyze particle shape, size, and size distribution [41]. SEM images of AgNPs have been depicted in Figure 8, the surface morphology of purified AgNPs was analyzed in different magnifications of 100000x, 60000x, 40000x, and 20000x. These photos suggest that the morphological structure of the AgNPs is that of spherical shapes ranging in size from 2.23 to 26.00 nm, with an average size of 8.77 nm. The scanning electron micrograph reveals the clustering and agglomerated spherical structure of AgNPs. Previously, the same kind of spherical-shaped AgNPs with their antibacterial activity was reported [42].

### 3.5. CV Analysis of AgNPs

The scavenger analysis is a good fit for the electrochemical method. The CV graph indicates the presence of oxidative and reductive active components in the solution mixture. The oxidation and reduction peaks were formed at different scan rates due to the electric scanning in the anodic and cathodic fields [43]. From the present study, in the anodic field, the two different oxidative peaks were developed at different scan rates, initially, the first peak was at 0.272 V, while another peak was at 0.418 V. From the reverse scanning, the reduction peak was formed in the cathodic current field at 0.03 V scan rate, as depicted in Figure 9. AgNPs of various sizes display various voltammetric

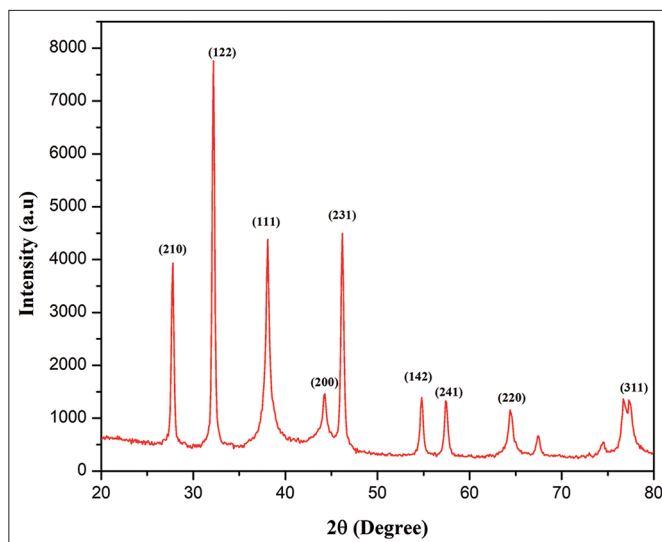


**Figure 7:** The XRD peaks pattern of green synthesized AgNPs.

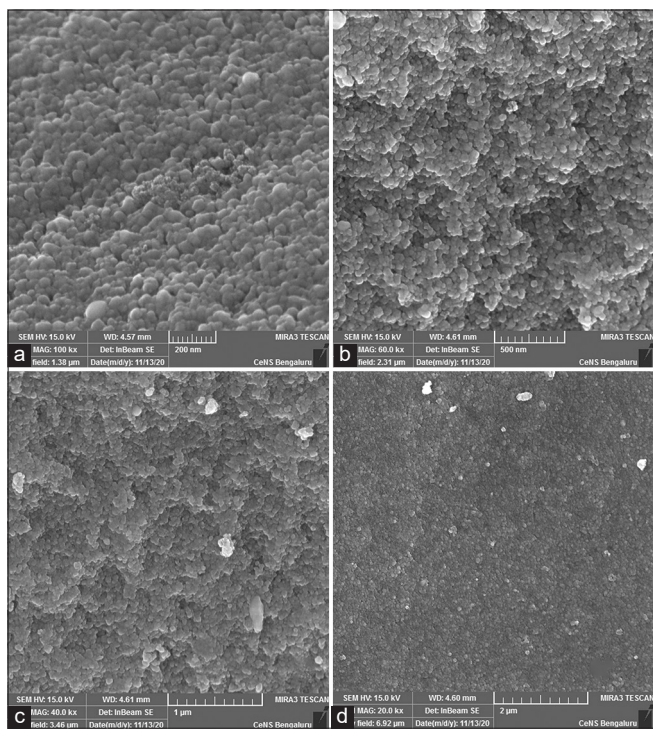


**Figure 8:** Scanning electron microscopic image of green synthesized AgNPs in various magnifications, (a)  $\times 100000$ , (b)  $\times 60000$ , (c)  $\times 40000$ , and (d)  $\times 20000$ .

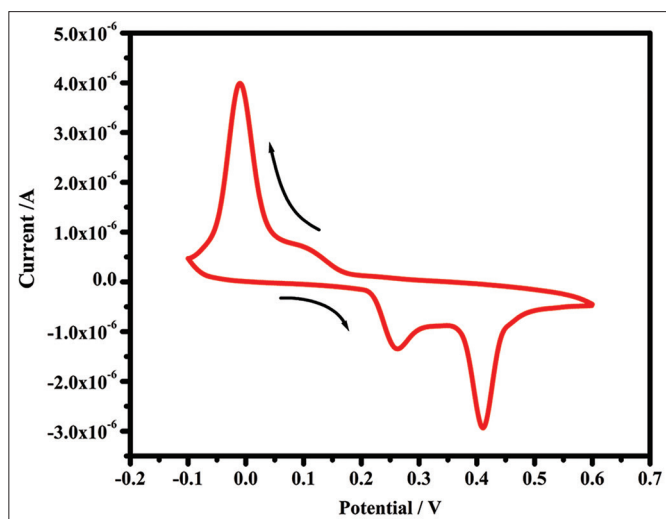


**Figure 9:** Cyclic voltammogram of synthesized silver nanoparticles.

profiles [44], and it indicates the presence of oxidative molecules in AgNPs and also acts as a good scavenger.

### 3.6. Antibacterial Effect of AgNPs

The biogenic AgNPs possessed more significant antibacterial activity because the particles were effective in killing both Gram-negative and Gram-positive bacteria [10]. The antibacterial activity was investigated against the pathogenic bacterial strains *S. aureus* MTCC (3160) (the Gram-positive bacteria) and *K. pneumoniae* MTCC (7407) (the Gram-negative bacteria) by well diffusion method shown in Figure 10. The AgNPs have reported a good zone of inhibition at

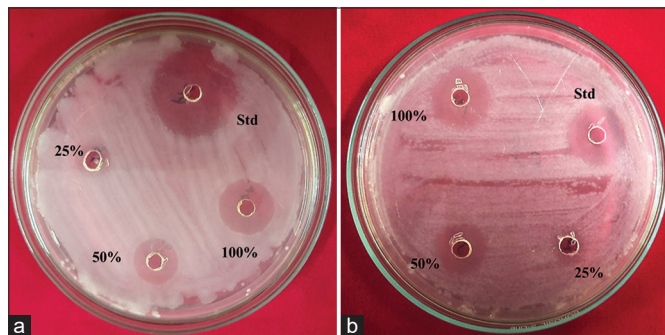


**Figure 10:** The silver nanoparticles show the zone of inhibition against *Staphylococcus aureus* MTCC (3160) and *Klebsiella pneumoniae* MTCC (7407).

**Table 2:** The XRD peaks and their corresponded planes.

Planes	Peak position	FWHM	Crystallite Size D nm	D nm average
210	27.77371	0.33604	24.35269392	
122	32.19819	0.34023	24.30283166	
111	38.09055	0.73274	11.46973509	
200	44.25411	1.81878	4.71519165	
231	46.2034	0.40488	21.33195467	17.28876937
142	54.80129	0.37771	23.69061963	
241	57.4615	0.40679	22.2710395	
220	64.4704	0.61704	15.22090018	
311	77.11085	1.23228	8.243958014	

different concentrations. Likewise, the standard drug Ampicillin reported  $18.33 \pm 1.15$  mm in *S. aureus* and about  $21.33 \pm 0.57$  mm in *K. pneumoniae*. The AgNPs at  $1000 \mu\text{g/ml}$  report  $15.33 \pm 0.57$  mm in *S. aureus* and about  $14.66 \pm 0.57$  mm of a zone of inhibition in *K. pneumoniae*. Because smaller AgNPs are directly linked to the bacterial cell wall and rapidly penetrate it, perhaps affecting cellular functions and leading to cellular death. Similar to this, AgNPs interact more competitively and effectively with their target pathogen because of their tiny size. According to several studies, Gram-positive bacteria's cell wall structure makes them more sensitive to the antibacterial capabilities of AgNPs than Gram-negative bacteria, additionally, AgNPs have shown enhanced antibacterial efficacy against many different types of bacteria, and fungi in a shape-dependent manner versus AgNPs with lower diameters (1–20 nm) and size [45]. The AgNPs implied the dimorphic transition in bacteria, the DNA lost its ability to replicate itself, and membranes were damaged, which stopped bacterial growth and development [46]. The zone of inhibition was varied and reported based on the concentrations and bacterial strains as shown in Table 3.

### 3.7. Cytotoxic Effect of AgNPs

The biogenic and green synthesized AgNPs show promising results in cancer cell apoptosis because the AgNPs might produce hazardous oxygen radicals, leading to genomic instability or DNA damage, and Cell death [47]. The cytotoxicity of synthesized AgNPs was conducted by MTT test against MCF-7 cell lines, the percentage of cell viability at various concentrations (1, 10, 50, 100, 200, and 400  $\mu\text{g/ml}$ ) of AgNPs is shown in Figure 11. The cytotoxicity effect of AgNPs is dose-dependent and shows good activity. About 51–44% of MCF-7 cells viability was reported at a concentration of 1–50  $\mu\text{g/ml}$ . With the concentration of quiring compound (AgNPs) in the range of 200 and 400  $\mu\text{g/ml}$ , the

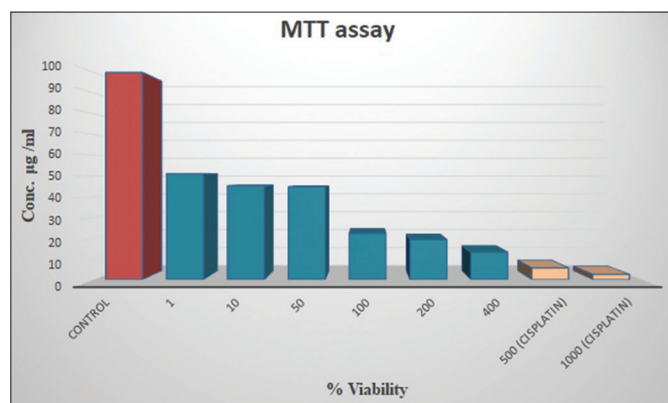


**Figure 11:** The silver nanoparticles show the cytotoxic activity against women's breast cancer (MCF-7) cell line.

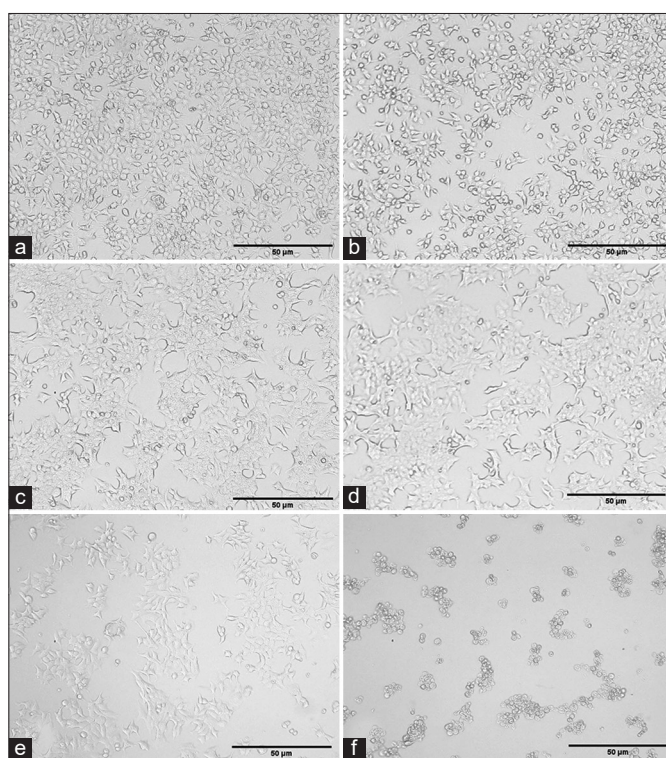


**Figure 12:** The cytomorphological variations of women's breast cancer cell lines: (a) Untreated, (b) 100 µg/ml, (c) 200 µg/ml, (d) 400 µg/ml, (e) Cisplatin 500 µg/ml, and (f) Cisplatin 1000 µg/ml.

**Table 3:** Antibacterial activity of silver nanoparticles against selected bacteria.

Concentration of AgNPs (µg/ml)	Zone of inhibition (mm) (mean of three replicates)	
	<i>Staphylococcus aureus</i>	<i>Klebsiella pneumoniae</i>
Standard (Std)	18.33±1.15	21.33±0.57
1000 (100%)	15.33±0.57	14.66±0.57
500 (50%)	11.66±0.57	11.66±0.57
250 (25%)	7.33±0.57	7.66±0.57

\*Standard (Std) concentration: 1000 µg/ml.

percentage of viability of MCF-7 decreased by about 19% and 13%. Likewise, the standard anticancer drug cisplatin was tested against the same cell lines in the range of 500 and 1000 µg/ml and showed 5.6 and 2.5% of cell viability. A similar previous study found that women's breast cancer cell lines exhibit considerable cytotoxic effects, the AgNPs with diameters ranging from 5 to 50 nm have effective inhibitory effects against the lymphoma Jurkat cell line, with an IC<sub>50</sub> value of 21.05 mg/mL [48]. The most likely reason was that the AgNP's size and shape led them to come into close contact with cell surfaces, causing cytotoxicity [49]. The cytomorphological variations caused by AgNPs on women's breast cancer cell lines at various concentrations (100, 200, 400 µg/ml, and Cisplatin 500 and 1000 µg/ml) involve an intracellular suicide program that possesses oxidative stress, cell shrinkage, coiling, and biochemical response that ultimately leads to cell death. These changes are depicted in Figure 12. The findings make it abundantly clear that the apoptosis rate of MCF-7 cell lines rises as the concentration of AgNPs increases. Because, from the synthesized AgNPs, the silver oxide ions released and interact strongly with cells, causing membrane breakage, damage occurs in DNA and RNA, and membrane disruption of lysosomal as well as reducing ATP and inactivating enzymes [50]. Like that the same thing was reported in the previous reports [51,52].

#### 4. CONCLUSION

In the present study, we analyzed the green synthesis of AgNPs for the first time, as well as their characterization. We also highlighted the antibacterial and cytotoxic properties of AgNPs produced using *H. ferruginea* leaf extract. The UV data's large peak absorption peak at 418 nm confirms that the extract of *H. ferruginea* converted AgNO<sub>3</sub> to AgNPs. The scanning electron microscope verified that the major nanoparticles were spherical in shape. The synthesized AgNPs reported promising antibacterial action against *K. pneumoniae* and *S. aureus*. The cytotoxic examination using the MTT assay on women's breast cancer cell lines revealed that AgNPs are a promising anticancer agent as normal cisplatin, nanoparticles have a significant death rate because their tiny size and spherical shape. The current research adds a unique and different approach to cancer treatment.

#### 5. AUTHORS' CONTRIBUTIONS

All authors made substantial contributions to conception and design, acquisition of data, or analysis and interpretation of data; took part in drafting the article or revising it critically for important intellectual content; agreed to submit to the current journal; gave final approval of the version to be published; and agreed to be accountable for all aspects of the work. All the authors are eligible to be an author as per the International Committee of Medical Journal Editors (ICMJE) requirements/guidelines.

#### 6. FUNDING

There is no funding to report.

#### 7. CONFLICTS OF INTEREST

The authors report no financial or any other conflicts of interest in this work.

#### 8. ETHICAL APPROVALS

This study does not involve experiments on animals or human subjects.

## 9. DATA AVAILABILITY

All data generated and analyzed are included in this research article.

## 10. PUBLISHER'S NOTE

This journal remains neutral with regard to jurisdictional claims in published institutional affiliation.

## REFERENCES

- Das J, Das MP, Velusamy P. *Sesbania grandiflora* leaf extract mediated green synthesis of antibacterial silver nanoparticles against selected human pathogens. *Spectrochim Acta A Mol Biomol Spectrosc* 2013;104:265-70.
- Guan Z, Ying S, Ofoegbu PC, Clubb P, Rico C, He F, *et al.* Green synthesis of nanoparticles: Current developments and limitations. *Environ Technol Innov* 2022;26:102336.
- Zhao X, Liu W, Cai Z, Han B, Qian T, Zhao D. An overview of preparation and applications of stabilized zero-valent iron nanoparticles for soil and groundwater remediation. *Water Res* 2016;100:245-66.
- Ajitha B, Reddy YA, Reddy PS. Biogenic nano-scale silver particles by *Tephrosia purpurea* leaf extract and their inborn antimicrobial activity. *Spectrochim Acta A Mol Biomol Spectrosc* 2014;121:164-72.
- Mukunthan KS, Balaji S. Cashew apple juice (*Anacardium occidentale* L.) speeds up the synthesis of silver nanoparticles. *Int J Green Nanotechnol* 2012;4:71-9.
- Khandel P, Yadaw RK, Soni DK, Kanwar L, Shahi SK. Biogenesis of metal nanoparticles and their pharmacological applications: Present status and application prospects. *J Nanostructure Chem* 2018;8:217-54.
- Hano C, Abbasi BH. Plant-based green synthesis of nanoparticles: Production, characterization and applications. *Biomolecules* 2021;12:31.
- Naganthran A, Verasoundarapandian G, Khalid FE, Masarudin MJ, Zulkharnain A, Nawawi NM, *et al.* Synthesis, characterization and biomedical application of silver nanoparticles. *Materials (Basel)* 2022;15:427.
- Erdogan O, Abbak M, Demirbolat GM, Birtekocak F, Aksel M, Pasa S, *et al.* Green synthesis of silver nanoparticles via *Cynara scolymus* leaf extracts: The characterization, anticancer potential with photodynamic therapy in MCF7 cells. *PLoS One* 2019;14:e0216496.
- Garibo D, Borbón-Núñez HA, de León JN, Mendoza EG, Estrada I, Toledano-Magaña Y, *et al.* Green synthesis of silver nanoparticles using *Lysiloma acapulcensis* exhibit high-antimicrobial activity. *Sci Rep* 2020;10:12805.
- Agarwal H, Kumar SV, Rajeshkumar S. A review on green synthesis of zinc oxide nanoparticles-An eco-friendly approach. *Resour Effic Technol* 2017;3:406-13.
- Srinivas CR, Kulkarni SB, Menon SK, Krupashankar DS, Iyengar MA, Singh KK, *et al.* Allergenic agent in contact dermatitis from *Holigarna ferruginea*. *Contact Dermatitis* 1987;17:219-22.
- Jadhav V, Kalase V, Patil P. GC-MS analysis of bioactive compounds in methanolic extract of *Holigarna grahamii* (wight) Kurz. *Int J Herb Med* 2014;2:35-9.
- Ravi A, Oommen PS. Phytochemical characterization of *Holigarna arnottiana* Hook. F. *J Pharm Res* 2012;5:3202-3.
- Adnan M, Chy MN, Kamal AM, Chowdhury KA, Rahman MA, Reza AA, *et al.* Intervention in neuropsychiatric disorders by suppressing inflammatory and oxidative stress signal and exploration of in silico studies for potential lead compounds from *Holigarna caustica* (Dennst.) Oken leaves. *Biomolecules* 2020;10:561.
- Uddin MZ, Rana MS, Hossain S, Ferdous S, Dutta E, Dutta M, *et al.* In vivo neuroprotective, antinociceptive, anti-inflammatory potential in Swiss albino mice and *in vitro* antioxidant and clot lysis activities of fractionated *Holigarna longifolia* Roxb. bark extract. *J Complement Integr Med* 2020;17.
- Panda SK, Das R, Mai AH, De Borggraeve WM, Luyten W. Nematicidal activity of *Holigarna caustica* (Dennst.) oken fruit is due to linoleic acid. *Biomolecules* 2020;10:1043.
- Lokapur V, Jayakar V, Divakar MS, Chalannavar RK, Lasrado L, Shantaram M. ZnO nanoparticles with spectroscopically controlled morphology, bioinspired from *Holigarna grahamii* (Wight) Kurz and delving its antioxidant and anticancer potential on A498 cell line. *Mater Today Commun* 2022;31:103338.
- Mitchell JD. The poisonous *Anacardiaceae* genera of the world. *Adv Econ Bot* 1990;8:103-29.
- Gamble JS. Flora of the Presidency of Madras. Vol. 1. London: West, Newman, and Adlard; 1921. p. 267-9.
- Doyle JJ, Doyle JL. A rapid DNA isolation procedure for small quantities of fresh leaf tissue. *Phytochem Bull* 1987;19:11-5.
- White TJ, Bruns T, Lee SJ, Taylor J. Amplification and direct sequencing of fungal ribosomal RNA genes for phylogenetics. *PCR Protoc Guide Methods Appl* 1990;18:315-22.
- Moodley JS, Krishna SB, Pillay K, Govender P. Green synthesis of silver nanoparticles from *Moringa oleifera* leaf extracts and its antimicrobial potential. *Adv Nat Sci Nanosci Nanotechnol* 2018;9:015011.
- Wan Mat Khalir WK, Shameli K, Jazayeri SD, Othman NA, Che Jusoh NW, Hassan NM. Biosynthesized silver nanoparticles by aqueous stem extract of *Entada spiralis* and screening of their biomedical activity. *Front Chem* 2020;8:620.
- Gagana SL, Kumaraswamy BE, Shivanna MB. Diversity, antibacterial and antioxidant activities of the fungal endophytes associated with *Schleichera oleosa* (Lour.) Merr. *S Afr J Bot* 2020;134:369-81.
- Elgrishi N, Rountree KJ, McCarthy BD, Rountree ES, Eisenhart TT, Dempsey JL. A practical beginner's guide to cyclic voltammetry. *J Chem Educ* 2018;95:197-206.
- Prasad R, Swamy VS. Antibacterial activity of silver nanoparticles synthesized by bark extract of *Syzygium cumini*. *J Nanopart* 2013;2013:1-6.
- Farhadi L, Mohtashami M, Saeidi J, Azimi-nezhad M, Taheri G, Khojasteh-Taheri R, *et al.* Green synthesis of chitosan-coated silver nanoparticle, characterization, antimicrobial activities, and cytotoxicity analysis in cancerous and normal cell lines. *J Inorg Organomet Polym Mater* 2022;32:1637-49.
- Saudah S, Zumaidar Z, Darusman D, Fitmawati F, Roslim, DI, Juliantari E. Molecular authentication of *Etilingera* spp. (*Zingiberaceae*) in Aceh Province, Indonesia using DNA barcoding. *Biodivers J Biol Divers* 2022;23:3976-83.
- Patil MP, Kim GD. Eco-friendly approach for nanoparticle synthesis and mechanism behind the antibacterial activity of silver and anticancer activity of gold nanoparticles. *Appl Microbiol Biotechnol* 2017;101:79-92.
- Jain D, Kachhwaha S, Jain R, Srivastava G, Kothari SL. Novel microbial route to synthesize silver nanoparticles using spore crystal mixture of *Bacillus thuringiensis*. *Indian J Exp Biol* 2010;48:1152-6.
- Dar MA, Ingle A, Rai M. Enhanced antimicrobial activity of silver nanoparticles synthesized by *Cryphonectria* sp. evaluated singly and in combination with antibiotics. *Nanomedicine* 2013;9:105-10.
- Lambert JB, Shurvell HF, Lightner DA, Cooks RG. Introduction to Organic Spectroscopy. New York: Macmillan Publishing Company; 1987.
- Awad TS, Moharram HA, Shaltout OE, Asker DY, Youssef MM. Applications of ultrasound in analysis, processing and quality control of food: A review. *Food Res Int* 2012;48:410-27.
- Haggag EG, Elshamy AM, Rabeh MA, Gabr NM, Salem M, Youssif KA, *et al.* Antiviral potential of green synthesized silver

- nanoparticles of *Lampranthus coccineus* and *Malephora lutea*. Int J Nanomed 2019;14:6217-29.
36. Veeraputhiran V. Bio-catalytic synthesis of silver nanoparticles. Int J Chem Tech Res 2013;5:2555-62.
  37. Annamalai J, Nallamuthu T. Green synthesis of silver nanoparticles: Characterization and determination of antibacterial potency. Appl Nanosci 2016;6:259-65.
  38. Basavegowda N, Idhayadhulla A, Lee YR. Tyrosinase inhibitory activity of silver nanoparticles treated with *Hovenia dulcis* fruit extract: An *in vitro* study. Mater Lett 2014;129:28-30.
  39. Rodríguez-Luis OE, Hernandez-Delgado R, Sánchez-Nájera RI, Martínez-Castañón GA, Niño-Martínez N, Sánchez Navarro MD, *et al.* Green synthesis of silver nanoparticles and their bactericidal and antimycotic activities against oral microbes. J Nanomater 2016;2016:1-10.
  40. Anigol LB, Charantimath JS, Gurubasavaraj PM. Effect of concentration and pH on the size of silver nanoparticles synthesized by green chemistry. Org Med Chem Int J 2017;3:1-5.
  41. Sadeghi B, Gholamhoseinpoor F. A study on the stability and green synthesis of silver nanoparticles using *Ziziphora tenuior* (Zt) extract at room temperature. Spectrochim Acta A Mol Biomol Spectrosc 2015;134:310-5.
  42. Ravindra S, Mohan YM, Reddy NN, Raju KM. Fabrication of antibacterial cotton fibres loaded with silver nanoparticles via "Green Approach". Colloids Surf A Physicochem Eng Aspects 2010;367:31-40.
  43. Jayaprakash N, Vijaya JJ, Kaviyarasu K, Kombaiah K, Kennedy LJ, Ramalingam RJ, *et al.* Green synthesis of Ag nanoparticles using *Tamarind* fruit extract for the antibacterial studies. J Photochem Photobiol B 2017;169:178-85.
  44. Giovanni M, Pumera M. Size-dependant electrochemical behavior of silver nanoparticles with sizes of 10, 20, 40, 80 and 107 nm. Electroanalysis 2012;24:615-7.
  45. Pallavi SS, Rudayni HA, Bepari A, Niazi SK, Nayaka S. Green synthesis of silver nanoparticles using *Streptomyces hirsutus* strain SNPGA-8 and their characterization, antimicrobial activity, and anticancer activity against human lung carcinoma cell line A549. Saudi J Biol Sci 2022;29:228-38.
  46. Dakal TC, Kumar A, Majumdar RS, Yadav V. Mechanistic basis of antimicrobial actions of silver nanoparticles. Front Microbiol 2016;7:1831.
  47. Chan EL, Zhang C, Cheung GS. Cytotoxicity of a novel nano-silver particle endodontic irrigant. Clin Cosmet Investig Dent 2015;7:65-74.
  48. Salehi S, Shandiz SA, Ghanbar F, Darvish MR, Ardestani MS, Mirzaie A, *et al.* Phytosynthesis of silver nanoparticles using *Artemisia marschalliana* Sprengel aerial part extract and assessment of their antioxidant, anticancer, and antibacterial properties. Int J Nanomed 2016;11:1835-46.
  49. Gliga AR, Skoglund S, Wallinder IO, Fadeel B, Karlsson HL. Size-dependent cytotoxicity of silver nanoparticles in human lung cells: The role of cellular uptake, agglomeration and Ag release. Part Fibre Toxicol 2014;11:11.
  50. Shukla RK, Sharma V, Pandey AK, Singh S, Sultana S, Dhawan A. ROS-mediated genotoxicity induced by titanium dioxide nanoparticles in human epidermal cells. Toxicol In Vitro 2011;25:231-41.
  51. Firdhouse MJ, Lalitha P. Apoptotic efficacy of biogenic silver nanoparticles on human breast cancer MCF-7 cell lines. Prog Biomater 2015;4:113-21.
  52. Rashidipour M, Heydari R. Biosynthesis of silver nanoparticles using extract of olive leaf: Synthesis and *in vitro* cytotoxic effect on MCF-7 cells. J Nanostruct Chem 2014;4:112.

**How to cite this article:**

Manjunath MK, Krishnamurthy YL. The physicochemical and biological properties of novel silver nanoparticles synthesized by the extract of *Hologarna ferruginea*. J App Biol Biotech. 2023;11(3):229-237. DOI: 10.7324/JABB.2023.109274